

Hybrid Projection For Encoding 360 VR Videos

Jintao Tang*

Xinyu Zhang†

Shanghai Key Laboratory of Trustworthy Computing, Shanghai, China
School of Computer Science & Software Engineering, East China Normal University, China

ABSTRACT

During the past five years, tons of economic 360 VR cameras (e.g., Ricoh Theta, Samsung Gear360, LG 360, Insta 360) are sold in the market. While 360 VR videos become ubiquitous very soon, 360 VR video standardization is still under discussion in the digital industry, and more concrete efforts are desired to accelerate its standardization and applications. Though ERP has been widely used for projection and packing layout while encoding 360 VR videos, it has severe projection distortion near poles. In this paper, we introduce a new format for encoding and storing 360 VR videos using hybrid cylindrical projection after thoroughly analyzing the problems with ERP. We show that our new hybrid format can minimize stretching distortion and generate well balanced pixel distribution in the resulting projection.

Index Terms: Computing methodologies—Computer graphics—Graphics systems and interfaces—Virtual reality

1 INTRODUCTION

Mobile virtual reality (VR) breakthrough creates a fast-growing demand for 3D immersive content. Compared to computer-generated content, 360 VR cameras [1, 4, 12, 14, 20] can rapidly capture immersive 360-degree VR videos by directly recording a surrounding environment in every direction at the same time. During playback, the viewer locates at the center of a spherical screen on which 360 VR videos are projected. 360 VR videos allow viewers feel actually in the midst of all the captured environment. There are many applications for 360 VR videos such as filming [2], live sports broadcasting [27], VR tourism [1], social communication [15], teleoperation in robotics [16, 19].

In the past few years, a few industrial leaders such as Google [1], Facebook [4] and Samsung [21], and a few new startups [12, 13] launched various 360 cameras. Tons of economic 360 VR cameras (e.g., Ricoh Theta, Samsung Gear360, LG 360, Insta 360 and more others) are sold in the market. While 360 VR videos become ubiquitous very soon, 360 VR video standardization is still under intensive discussion and concrete efforts are urgently desired to bridge the standardization gap in the digital industry.

In order to support efficient storage, access and processing, a 360 video requires to be projected onto a 2D domain (i.e., a transformation from a spherical surface to a plane) and stored in conventional video format. Among these projections, Equi-Rectangular Projection (ERP) [23] is widely used in gaming industry and 360 videos. Due to projection distortion, a sphere may be sampled with different density across the entire surface. For example, ERP over-samples the sphere near poles, which results in higher density at the top and bottom of a rectangular frame than other regions. ERP and their corresponding storage format exhibit imbalanced pixel density.

Main Results: In this paper, we thoroughly analyze the problems with ERP. Based on our analysis, we propose a new format for

encoding and storing 360 VR videos using hybrid cylindrical projection. Our new format can generate well balanced pixel distribution and minimize stretching ratios in the resulting projection. Due to its simplicity, we believe our work will contribute to the ongoing standardization efforts towards efficient storage format for 360 VR videos.

2 RELATED WORK

Projections are extensively studied in cartography [22], surface parameterization [7], tiling [10] and computer graphics [18, 26]. Here, we briefly review some related work. For more details on theoretical aspects of projection or parameterization, we refer to the surveys by Floater [7] and Snyder [22].

For 360 videos, all the existing projections associate a spherical surface with simple planar domains like rectangles, squares or triangles. A projection generates a bijective mapping that maps a point of the spherical surface onto the one on the planar domain. Among these projections, Equi-Rectangular Projection (ERP) [23] has been widely used in gaming industry and cartography. This projection unfolds and flattens a sphere into a 2D rectangle. Cubemap Projection (CMP) [9] is another frequently used method. It deforms a sphere into a cube and flattens a 1/6 spherical surface into a cube's face. Then the cube's six faces are unfolded and packed onto a rectangle. A straightforward deformation is to embed the sphere in a cube and project the spherical surface outwards onto the cube's faces. CMP offers better pixel uniformity than ERP. A few variations like Google's Equi-Angular Cubemap (EAC) [8] were also suggested. EAC further reduces projection distortion. Both CMP and EAC use six squares for bijective mapping and have been used in 360 videos by Google. The work in [11] used two stages to perform uniform mapping. Other methods use more complex domains for projections, such as Compact Octahedron Projection (COHP) [5, 17] and Compact Icosahedron Projection (CISP) [6]. COHP and CISP project spherical triangular surfaces onto planar triangular domains. COHP uses eight triangles and CISP uses twenty triangles. However, due to its sophisticated bijective mapping and a large number of internal packing edges, it is not clear if CISP is useful in practice.

3 CYLINDRICAL PROJECTION

Our goal is to build a map between a sphere and a rectangle while minimizing distortions and maintaining evenly distributed pixel density. The main idea is to find an appropriate mapping function between a planar rectangle and a spherical surface (see Figure 1). A good projection will allow us to generate high quality 360 VR videos. Here, we denote a point on the spherical surface as (θ, φ) with longitude θ and latitude φ , and a corresponding point on the uv projection rectangle as (u, v) . A general explicit projection form is given below.

$$\begin{cases} u = F(\theta, \varphi) \\ v = G(\theta, \varphi) \end{cases}$$

3.1 Stretching Ratio

We will use two metrics: Area Stretching Ratio (ASR) [24] and Linear Stretching Ratio (LSR) to measure projection distortion. Note

*e-mail: todd.j.tang@gmail.com

†Corresponding author. e-mail:xyzhang@sei.ecnu.edu.cn

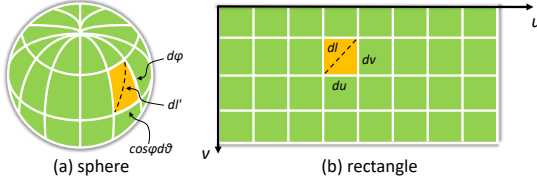


Figure 1: The LSR and ASR of two corresponding surfaces.

that any projection has distortions. As shown in Figure 1, we define ASR as

$$\text{ASR} = \frac{\delta \text{AREA}(\theta, \varphi)}{\delta \text{AREA}(u, v)} = \frac{\cos \varphi |d\theta d\varphi|}{dudv} = \frac{\cos \varphi}{J(\theta, \varphi)} \quad (1)$$

where $\delta \text{AREA}(\cdot)$ is the surface area at a specified point and J is the Jacobian determinant of F and G

$$J = \begin{vmatrix} \frac{\partial F}{\partial \theta} & \frac{\partial F}{\partial \varphi} \\ \frac{\partial G}{\partial \theta} & \frac{\partial G}{\partial \varphi} \end{vmatrix} \quad (2)$$

In addition, we define Linear Stretching Ratio (LSR) as

$$\text{LSR} = \frac{dl'}{dl} = \frac{\sqrt{(d\varphi)^2 + (\cos \varphi d\theta)^2}}{\sqrt{du^2 + dv^2}} \quad (3)$$

Consider that

$$du = \frac{\partial F}{\partial \theta} d\theta + \frac{\partial F}{\partial \varphi} d\varphi \quad (4)$$

$$dv = \frac{\partial G}{\partial \theta} d\theta + \frac{\partial G}{\partial \varphi} d\varphi \quad (5)$$

LSR can be derived and written as

$$\text{LSR} = \sqrt{\left(\frac{\partial F}{\partial \theta}\right)^2 + \left(\frac{\partial G}{\partial \theta}\right)^2} \cdot \frac{1}{r} \quad (6)$$

where $r = \cos \varphi$ is the radius of the latitude circle for a unit sphere.

Intuitively, the same number of pixels will be used to store a feature on a spherical surface, no matter where the feature is located. For instance, if a feature on the spherical surface occupies a given number of pixels, it should only require the same number of pixels of storage in the planar rectangle after projection. Any more is a waste of space and bandwidth, and any less reduces image quality. ASR and LSR respectively evaluate two dimensional and one dimensional distortions that cause the pixel spacing uneven. As shown in Figure 3, both ASR and LSR increases away from equator and research to extreme in polar regions, which indicates that pixels at equator space more evenly than those near poles.

3.2 Cylindrical Projections

We use two cylindrical projections: regular Equi-Rectangle Projection (ERP) and Transverse Cylindrical Projection (TCP) to generate a hybrid projection. Both ERP and TCP belong to the category of cylindrical projection family, in which the projection wraps the sphere with a tangent cylinder and maps the spherical surface to a rectangle. Intuitively, ERP unfolds a vertically ‘standing’ cylinder and then wraps the sphere. Since adjacent longitudes have the same distance, ERP is also called Equidistant Cylindrical Projection. TCP unfolds a horizontally ‘lying’ cylinder in the constraint of area-preserving. The regular cylindrical projection (i.e., ERP) is illustrated in Figure 2 and the axis of the cylinder in TCP lies in the equatorial plane.

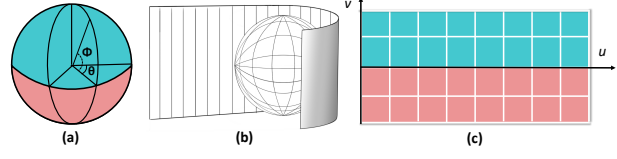


Figure 2: Spherical projection used in encoding 360 VR videos. (a) spherical surface; (b) cylindrical projection process and (c) rectangular uv projection plane.

ERP and TCP show different performances in terms of ASR and LSR. By taking their respective advantages, we can obtain better performance than each individual projection. We give a detailed analysis as follows.

3.2.1 ERP

ERP has the simplest form formulated in Eq. (7).

$$\begin{cases} u = \theta \\ v = \varphi \end{cases} \quad (7)$$

From Eqs. (6) and (7), its LSR is derived as

$$\text{LSR}_{\text{ERP}} = \frac{1}{\cos \varphi} \quad (8)$$

As a result, LSR_{ERP} varies with respect to the latitude φ . From Eq. (1) and Eq. (7), we derive that $J_{\text{ERP}} = 1$, and then we have

$$\text{ASR}_{\text{ERP}} = \cos \varphi. \quad (9)$$

3.2.2 TCP

When using a transverse cylinder, we formulate an equal-area TCP as

$$\begin{cases} u = \cos \varphi \sin \theta \\ v = \arctan \left(\frac{\tan \varphi}{\cos \theta} \right) \end{cases} \quad (10)$$

Using Eqs. (6) and (10), we derive its LSR shown below

$$\text{LSR}_{\text{TCP}} = \frac{1}{\cos \varphi} \cdot \sqrt{\left[\frac{\tan^2 \varphi \sin^2 \theta}{(\tan \varphi + \cos^2 \theta)^2} + \cos^2 \varphi \cos^2 \theta \right]} \quad (11)$$

This is a function of longitude θ and latitude φ . From Eq. (10), we have

$$J_{\text{TCP}} = \cos \varphi \cdot \frac{\cos^2 \varphi \cos^2 \theta + \sin^2 \varphi}{\sin^2 \varphi \sin^2 \theta + \cos^2 \theta} = \cos \varphi \quad (12)$$

As a result, its ASR can be computed using Eq. (13), which is a constant of 1.

$$\text{ASR}_{\text{TCP}} = \frac{\cos \varphi}{J_{\text{TCP}}} = 1 \quad (13)$$

For intuitive analysis, we plot these functions: LSR_{ERP} , ASR_{ERP} and LSR_{TCP} given in Eqs.(8), (9) and (11), respectively. As shown in Figure 3, both LSR_{ERP} and ASR_{ERP} are cosine functions with respect to latitude φ . Their stretching ratios are acceptable near equator (i.e., $|\varphi| \leq \varphi_t$, where φ_t is a specified threshold). Our TCP is an area-preserving projection (i.e., $\text{ASR} = 1$). $\text{LSR}_{\text{TCP}} \approx 1$ for specified latitude φ ($|\varphi| \geq \varphi_t$). Intuitively speaking, the regular ERP has good performance around equator while TCP has good performance near poles. Note that ASR_{TCP} is a constant.

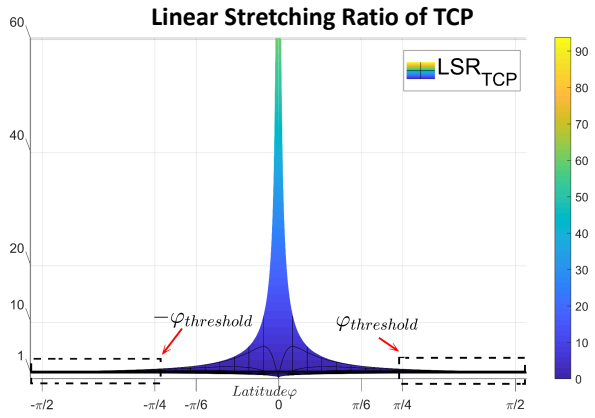
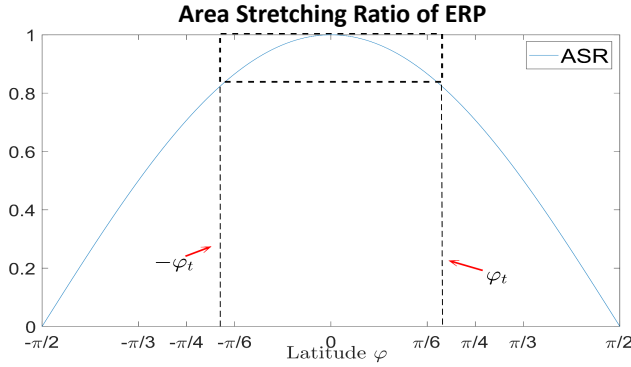
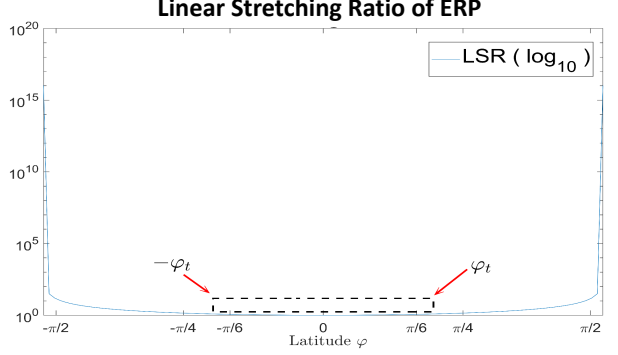


Figure 3: The function graphs of LSR_{ERP} (top), ASR_{ERP} (middle) and LSR_{TCP} (bottom). Note that the graph of ASR_{TCP} is not shown here since $ASR_{TCP} = 1$.

4 HYBRID PROJECTION

4.1 Latitude Threshold

Based on the analysis of ERP and TCP in Section 3, we define the projection latitude threshold φ_t to combine the two cylindrical projections into one hybrid projection, as shown in Figure 4.

In order to generate a compact form, the key is to choose the value φ_t . Here, we introduce two possible values: $\pi/4$ and $\pi/6$, making the frame-packing simple and easy. While $\varphi_t = \pi/4$, the resulting hybrid projection combines equal latitude of ERP and TCP, which is an intuitive hybrid combination of both ERP and TCP. While $\varphi_t = \pi/6$, the resulting hybrid projection discards more polar regions of ERP that exhibits the most distortions, and retains more polar regions of TCP that preserves area, yet has more distortion

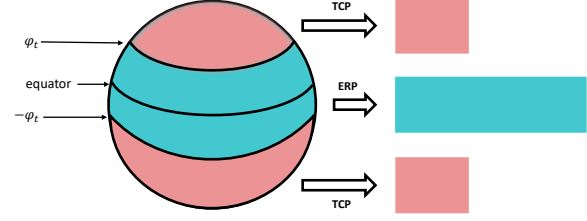


Figure 4: Hybrid Projection

in terms of LSR metric. Table 1 shows the range of stretching ratios for latitude threshold φ_t . Table 2 lists the stretching ratios of ERP, CMP [9], TCP, SUM [11], EAC and our hybrid methods. Without prejudice to the results, the lower bounds are scaled to 1.00. Therefore, the smaller upper bound yields the lower projection distortion.

Table 1: Stretching ratio range for latitude threshold φ_t

φ_t	LSR_{ERP}	LSR_{TCP}	ASR_{ERP}	ASR_{TCP}
$\pi/4$	[1.00, 1.41]	[0.95, 1.41]	[0.70, 1.00]	1
$\pi/6$	[1.00, 1.16]	[0.90, 2.00]	[0.87, 1.00]	1

Table 2: Stretching ratio ranges for ERP, CMP [9], TCP, SUM [11], EAC [8] and our hybrid methods.

	LSR	ASR
ERP	[1.00, $+\infty$]	[1.00, $+\infty$]
CMP	[1.00, $+\infty$]	[1.00, $+\infty$]
TCP	[1.00, $+\infty$]	[1.00, 1.00]
SUM	[1.00, $+\infty$]	[1.00, 1.00]
EAC	[1.00, $+\infty$]	[1.00, 1.41]
Our Hybrid($\pi/4$)	[1.00, 1.48]	[1.00, 1.41]
Our Hybrid($\pi/6$)	[1.00, 2.23]	[1.00, 1.15]

4.2 Frame Packing Layouts

Here, we propose three frame-packing layouts for the hybrid projection while adopting the two φ_t values. The width-to-height aspect ratios are given in Table 3.

Table 3: Width-to-height ratios of three frame-packing layouts under hybrid projection

Frame-Packing Layout	φ_t	Width-to-Height Ratio
A	$\pi/4$	6.83
B	$\pi/4$	1.71
C	$\pi/6$	4.10

As shown in Figure 5, frame-packing layout A for $\varphi_t = \pi/4$ is similar to Segmented Sphere Projection [28] and it has 2 packing seams indicated by red dash lines. The width-to-height ratio is 6.83. Frame-packing layout B for $\varphi_t = \pi/4$ divides both ERP and TCP into eastern and western hemispheres, and stitches them into 4 discontinuous regions, making the hybrid projection 4 packing seams. The width-to-height ratio is 1.71, which is very close to industrial standard aspect ratio 16:9. Frame-packing layout C for $\varphi_t = \pi/6$ stitches four segments with 3 packing seams. Its width-to-height ratio is 4.10.

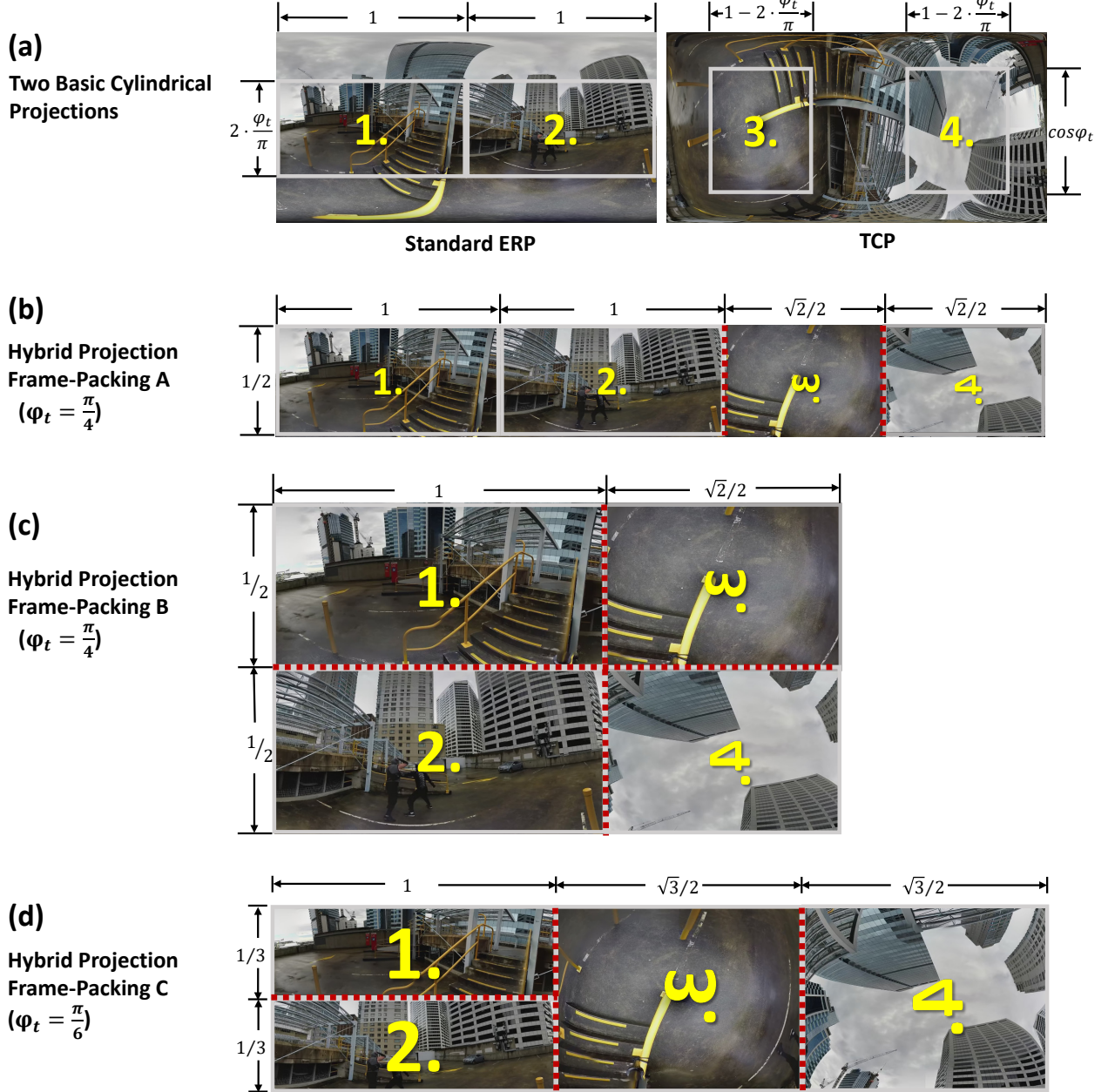


Figure 5: Compact Frame-packing Layouts for Hybrid Projection. (a): Given two basic cylindrical projections ERP and TCP. (b) Frame-packing layout A with $\varphi_t = \pi/4$ and width-to-height ratio 6.83. (c) Frame-packing layout B with $\varphi_t = \pi/4$ and width-to-height ratio 1.71. (d) Frame-packing layout C with $\varphi_t = \pi/6$ and width-to-height ratio 4.10.

5 EXPERIMENTS AND RESULTS

To demonstrate performances of hybrid projection and frame-packing layouts described in Section 4, we conducted extensive experiments of quality of evaluation (QoE). We also show the computational costs of different projections and frame-packing layouts.

5.1 Discontinuity, Distortion and Pixel Density

To perform intuitive comparison, we use discontinuity graph, distortion graph and pixel density graph to present the performance of hybrid projection.

As shown in the first row of each graph in Figure 6, we use a color striped texture to illustrate discontinuity in resulting packing

layouts. Textures are preserved very well while discontinuity merely occurs at the packing edges. The second row of each graph is designed to demonstrate area distortion during projection. A given number of red dots in the same size are evenly spreading on a spherical surface. A good projection minimizes distortion by preserving projection areas. Thanks to the advantages of both ERP and TCP, the distortion of hybrid projection is well controlled. The results shown in Figure 6 confirms our analysis given in Table 2. From the pixel density in the third row of each graph in Figure 6, we observe that pixel density at equator is well preserved using ERP format, and the polar regions are condensed using TCP format.

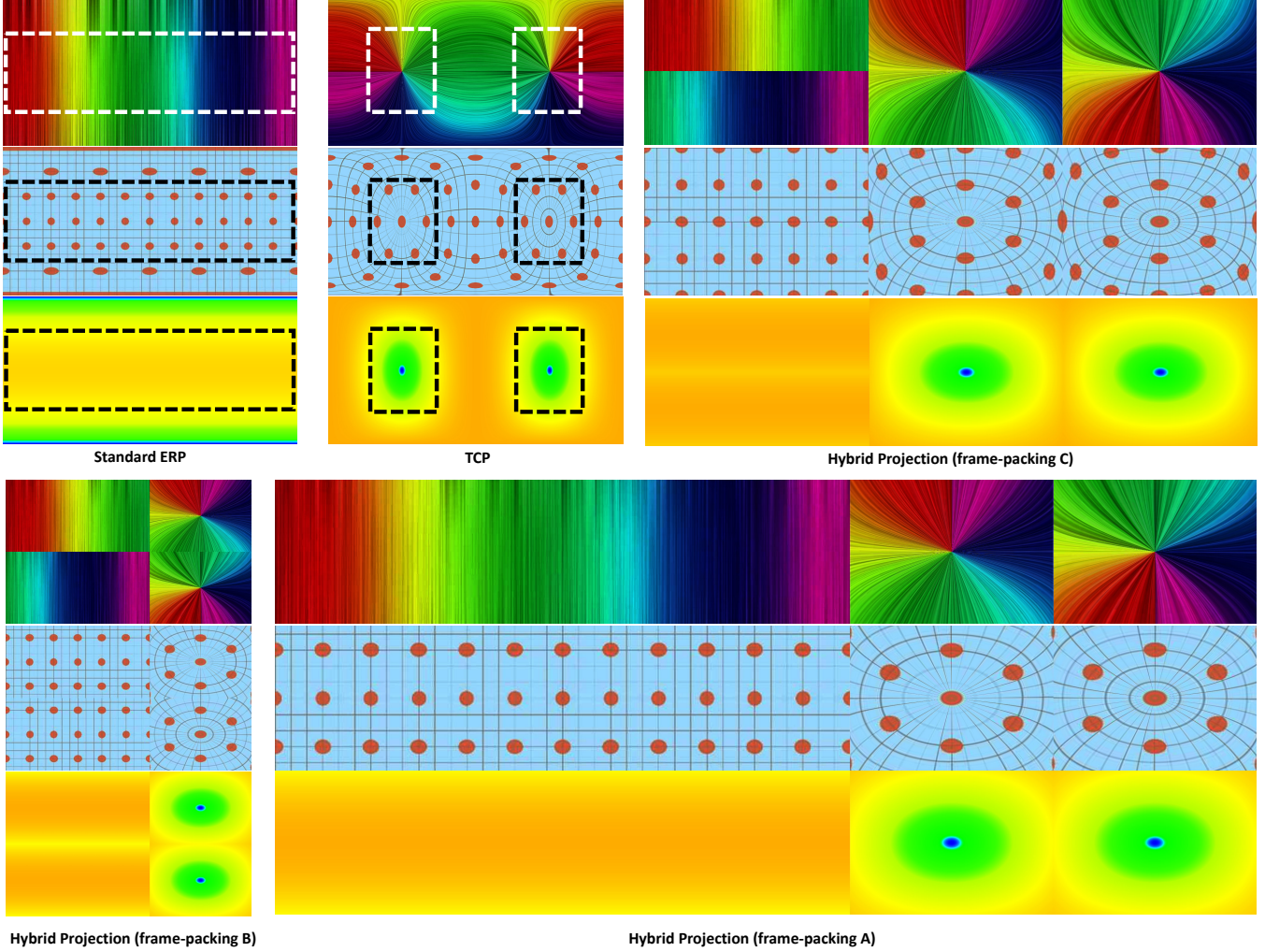


Figure 6: QoE of Projections, (a)(b) are two basic cylindrical projections ERP and TCP. (c)(d)(e) are three frame-packing layouts under hybrid projections. The top, middle and bottom graphs from (a) to (e) is to demonstrate discontinuity, distortion and pixel density.

5.2 PSNR & BD-rate

Peak signal-to-noise ratio (PSNR) has been widely used to perform objective QoE for image/video sequences. However, for 360 VR videos, since pixels are located on a spherical surface, it is non-trivial to evaluate spherical images/videos using PSNR. Spherical-PSNR (S-PSNR) [25] was proposed to evaluate omnidirectional video content, and Craster Parabolic Projection PSNR (CPP-PSNR) [25] was suggested to evaluate distortions. Each type of PSNR has three metrics suggested in [29], also shown in Table 4. Here we applied Cross Format type and End-to-End type of S-PSNR and CPP-PSNR to evaluate the process of projections.

Table 4: PSNR Metrics Used for Objective QoE

Name	Evaluate Process
CodeC	Encode/Decode
Cross Format	Forward conversion, Encode/Decode
End-to-End	Forward/Inverse format conversion, Encode/Decode

We used four test sequences for video encoding and projection after converting them into six different resolution levels listed in

Table 5. Then their PSNRs are calculated.

To make comparisons between PSNR/Bitrate curves, we use the method suggested by Bjontegaard [3] to calculate the BD-rate. The BD-rate calculates an average reduction among different PSNR values. Intuitively, for an given PSNR value, the smaller a video's bitrate is, the better quality it has. We take a few PSNR values of different bitrates for two videos and then we use linear interpolation to perform regression between these PSNRs and bitrate values. We average the bitrate reductions (BD-rate) and compare them against standard ERP. The comparison between individual projections are plotted in Figure 7.

Among these three frame-packing layouts using hybrid projection, the majority of BD-rate reductions on Cross-Format S-PSNR and CPP-PSNR, End-to-End S-PSNR and CPP-PSNR reaches to 5%, as shown in Figure 7. This shows that our hybrid projection has better performance compared with the regular ERP. More specifically, hybrid projection frame-packing B has the most significant BD-rate reductions. We also show the comparison with other techniques such as EAC [8] and SUM [11]. Figure 8 shows more results for video sequences using three hybrid projections and frame-packing layouts.

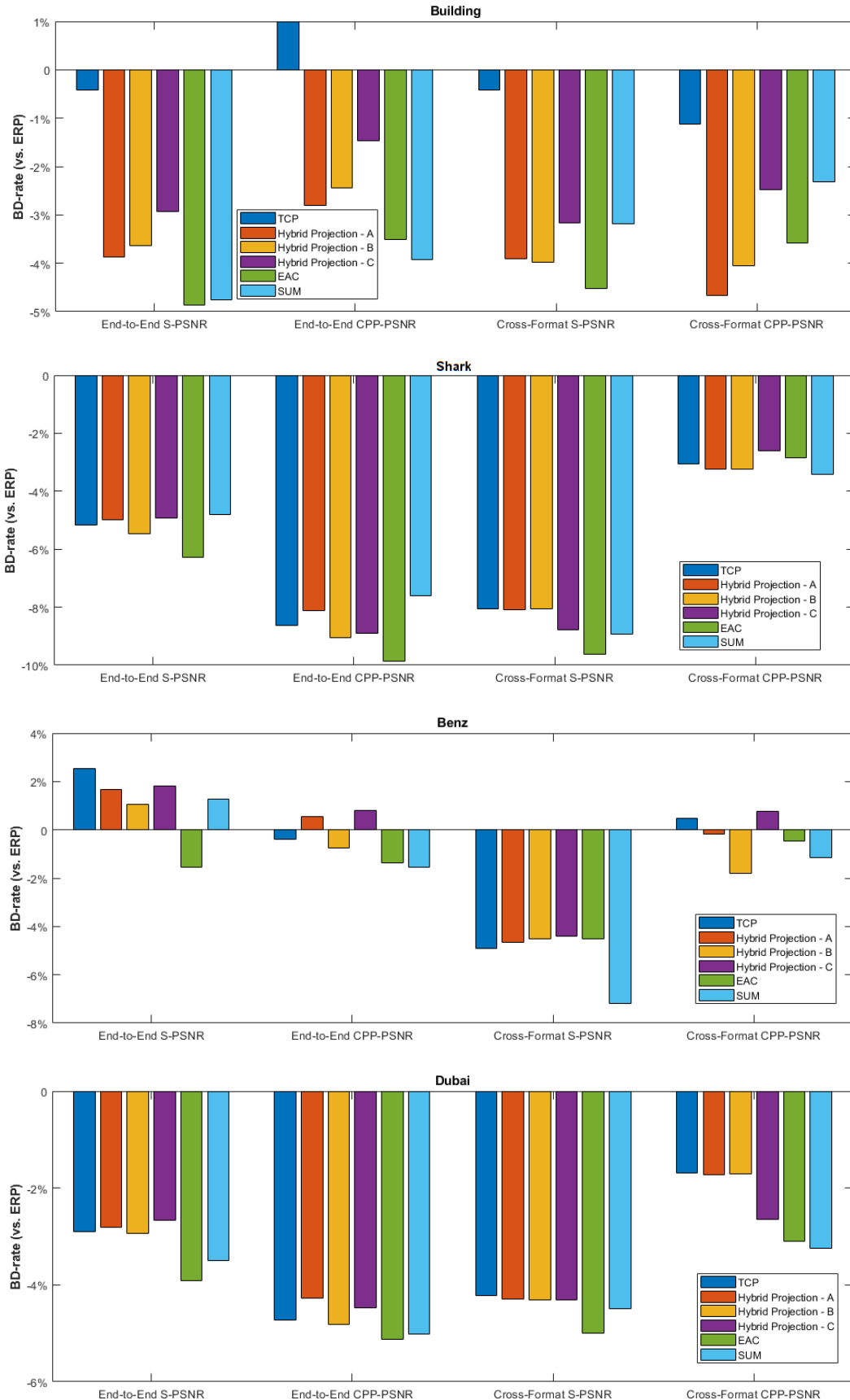


Figure 7: BD-rate reduction of different projections and packing layouts compared against standard ERP.

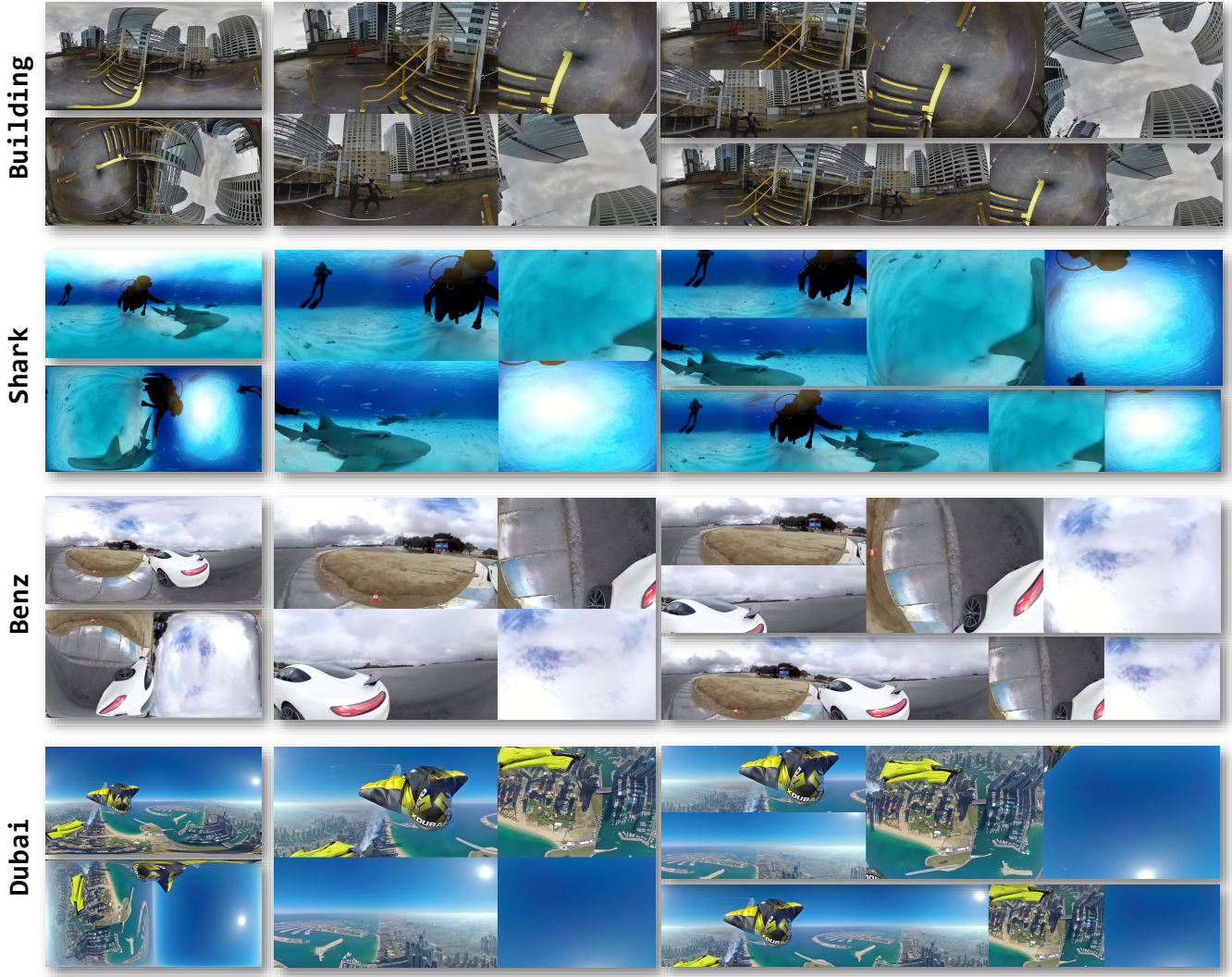


Figure 8: Standard ERP (left-top), TCP (left-bottom) and Hybrid projection (Frame-packing A: right-bottom, Frame-packing B: middle, Frame-packing C: right-top) graphs of test sequences.

5.3 Computational Costs

We evaluate computational performance during video hybrid projection conversions. We use four video sequences to test the performance of 360 video encoding and projection. The timings are measured on a PC with a i7-6700 CPU under Windows.

Table 5: Average computation time for hybrid projections.

Resolution Level	ERP	TCP	Hybrid-A	Hybrid-B	Hybrid-C
384 × 192	43.0s	43.0s	41.5s	44.2s	44.3s
768 × 384	86.3s	87.1s	85.3s	87.2s	85.6s
1152 × 576	149.4s	151.2s	145.9s	149.2s	146.1s
1536 × 768	226.9s	231.6s	230.7s	227.5s	227.2s
1920 × 960	319.5s	327.6s	329.1s	320.4s	320.7s
2304 × 1152	426.6s	443.8s	441.1s	431.9s	431.8s

As shown in Table 5, it is obvious that ERP is fastest due to its simplicity, while TCP is slower than others. Hybrid projections lie between ERP and TCP.

6 CONCLUSIONS AND FUTURE WORK

We present an efficient 360 video format using hybrid cylindrical projection. This format takes the advantages of regular ERP around equator area and TCP near poles. Hence, it can provide a better performance at the polar area than ERP by combining with TCP. Meanwhile, this new format can effectively control area stretching and linear stretching ratios. Among the three hybrid projection packing layout, frame-packing B shows good BD-rate reductions while maintaining a width-to-height ratio close to the industrial standard aspect ratio 16:9. Due to its simplicity, we expect our work will contribute to the ongoing standardization efforts towards efficient storage format for 360 VR videos. We expect this work can inspire more research along this direction.

Our frame-packing layouts has discontinuous edges. For a highly compressed video, some artifacts may occur to the packing seams. However, the artifacts can be reduced using padding techniques. In future work, we would like to investigate other techniques like conformal projection to further improve projection efficiency. In addition, some optimization techniques such as parallel computation, GPU-acceleration and edge padding, can be used to further speed up the entire performance.

ACKNOWLEDGMENTS

This work was supported by the NSFC (No.61631166002, No.61572196). The authors wish to thank Wensong Li and Nikk Mitchell from FXG VR for helpful discussion.

REFERENCES

- [1] R. Anderson, D. Gallup, J. T. Barron, J. Kontkanen, N. Snavely, C. Hernández, S. Agarwal, and S. M. Seitz. Jump: Virtual Reality Video. *ACM Transactions on Graphics*, 35(6):198:1–198:13, Nov. 2016.
- [2] S. S. Bhadsavle, X. H. S. Yap, J. Segler, R. Jaisimha, N. Raman, Y. Feng, S. J. Biggs, M. Peoples, R. B. Brenner, and B. C. McCann. Immerj: A novel system for democratizing immersive storytelling. In *IEEE Virtual Reality*, 2017.
- [3] G. Bjontegaard. Calculation of average PSNR differences between RD-curves. Technical report, Video Coding Experts Group (VCEG) M33, ITU-T, Apr. 2001.
- [4] B. K. Cabral. Introducing Facebook Surround 360: An open, high-quality 3D-360 video capture system, 4 2016.
- [5] T. Engelhardt and C. Dachsbacher. Octahedron environment maps. In *VMV*, pp. 383–388, 2008.
- [6] I. Fisher. A world map on a regular icosahedron by gnomonic projection. *Geographical Review*, 33(4):605–619, 1943.

- [7] M. Floater and K. Hormann. *Advances in Multiresolution for Geometric Modelling*, chap. Surface Parameterization: A Tutorial and Survey. Springer, Berlin, Heidelberg, 2005.
- [8] Google. Bringing pixels front and center in VR video, 2017.
- [9] N. Greene. Environment mapping and other applications of world projections. *IEEE Computer Graphics and Applications*, 6(11):21–29, 1986.
- [10] B. Grünbaum and G. C. Shephard. *Tilings and Patterns*. W. H. Freeman & Co., New York, NY, USA, 1986.
- [11] J. Guo, Q. Pei, G. Ma, L. Liu, and X. Zhang. A new uniform format for 360 VR videos. In *Pacific Graphics*, pp. 245–254, 2018.
- [12] Insta. Insta360 Camera, 2018.
- [13] Jaunt. JauntVR:Jaunt ONE, 2018.
- [14] R. Konrad, D. G. Dansereau, A. Masood, and G. Wetzstein. SpinVR: Towards live-streaming 3D virtual reality video. *ACM Transactions on Graphics*, 36(6):209:1–209:12, Nov. 2017.
- [15] H. Lee, G. Ha, S. Lee, and S. Kim. A mixed reality tele-presence platform to exchange emotion and sensory information based on MPEG-V standard. In *IEEE Virtual Reality*, 2017.
- [16] S. Livatino. VR enhanced teleoperation. In *International Conference on Artificial Reality and Telexistence*, 2007.
- [17] E. Praun and H. Hoppe. Spherical parametrization and remeshing. In *ACM Transactions on Graphics*, vol. 22, pp. 340–349. ACM, 2003.
- [18] B. Purnomo, J. D. Cohen, and S. Kumar. Seamless texture atlases. In *Eurographics/SIGGRAPH Symposium on Geometry Processing*, pp. 65–74, 2004.
- [19] T. Rhee, L. Petikam, B. Allen, and A. Chalmers. Mr360: Mixed reality rendering for 360 panoramic videos. *IEEE Transactions on Visualization and Computer Graphics*, 23(4):1379–1388, 2017.
- [20] RICOH. RICOH THETA, 2018.
- [21] Samsung. Samsung Gear360, 2018.
- [22] J. P. Snyder. *Map projections—A working manual*, vol. 1395. US Government Printing Office, 1987.
- [23] J. P. Snyder. *Flattening the earth: two thousand years of map projections*. University of Chicago Press, 1997.
- [24] Y. Sun, A. Lu, and L. Yu. Weighted-to-spherically-uniform quality evaluation for omnidirectional video. *IEEE Signal Processing Letters*, 24(9):1408–1412, Sept 2017. doi: 10.1109/LSP.2017.2720693
- [25] E. A.-A. S. V. Zakharchenko, A. Dsouza. AhG8: Suggested testing procedure for 360-degree video. Technical report, Joint Video Exploration Team of ITU-T SG16 WP3 and ISO/IEC JTC1/SC29/WG11, Oct. 2016.
- [26] F. M. Weinhaus and V. Devarajan. Texture mapping 3D models of real-world scenes. *ACM Computer Survey*, 29(4):325–365, Dec. 1997.
- [27] F. Xu, T. Zhao, B. Luo, and Q. Dai. Generating VR live videos with tripod panoramic rig. In *IEEE Virtual Reality*, pp. 31–36, 2018.
- [28] J.-L. Ya-Hsuan Lee, HungChih Lin. EE4: ERP/EAP-based segmented sphere projection with different padding sizes. Technical report, Joint Video Exploration Team of ITU-T SG16 WP3 and ISO/IEC JTC1/SC29/WG11, Oct. 2016.
- [29] J. B. Yan Ye, Elena Alshina. Algorithm descriptions of projection format conversion and video quality metrics in 360Lib version 5. Technical report, Joint Video Exploration Team of ITU-T SG16 WP3 and ISO/IEC JTC1/SC29/WG11, Oct. 2017.